**American Journal of Chemical Engineering**
2020; 8(4): 76-89
http://www.sciencepublishinggroup.com/j/ajche
doi: 10.11648/j.ajche.20200804.11
ISSN: 2330-8605 (Print); ISSN: 2330-8613 (Online)

# Economical Synthesis of High Surface Area γ-$Al_2O_3$ for the Adsorption of Organic Pollutant from Wastewater

**Jinjin Li[1, 2], Hao Wang[3], Ronghai Zhu[1, 2], Honggang Chang[1, 2], Gang Xiong[1, 2], Jingxian Wu[3], Hao Feng[3], Ping Li[3, *]**

[1]Research Institute of Natural Gas Technology, PetroChina Southwest Oil & Gasfield Company, Chengdu, China

[2]National Energy R&D Center of High Sulfur Gas Exploitation, Chengdu, China

[3]State Key Laboratory of Chemical Engineering, East China University of Science and Technology, Shanghai, China

## Email address:

li_jj@petrochina.com.cn (Jinjin Li), lipingunilab@ecust.edu.cn (Ping Li)

[*]Corresponding author

## To cite this article:

Jinjin Li, Hao Wang, Ronghai Zhu, Honggang Chang, Gang Xiong, Jingxian Wu, Hao Feng, Ping Li. Economical Synthesis of High Surface Area γ-$Al_2O_3$ for the Adsorption of Organic Pollutant from Wastewater. *American Journal of Chemical Engineering.* Vol. 8, No. 4, 2020, pp. 76-89. doi: 10.11648/j.ajche.20200804.11

**Received**: July 25, 2020; **Accepted**: August 8, 2020; **Published**: August 25, 2020

**Abstract:** A series of γ-$Al_2O_3$ with high surface area applied for removal of Congo red (CR) from aqueous solution was prepared from cheap inorganic aluminum precursor using simple precipitation method in presence of an inexpensive anionic surfactant (sodium dodecyl sulfate, SDS). The material characterization by several techniques revealed that SDS plays an important role on the morphology and textural properties of the resultant γ-$Al_2O_3$, and the largest surface area of γ-$Al_2O_3$ (416.65 $m^2/g$) was obtained by varying molar ratio of SDS to aluminum precursor to be 0.375. The CR adsorption experiments identified that the adsorption isotherms on the as-synthesized γ-$Al_2O_3$ obey the Langmuir model. The maximum CR adsorption capacity of 831.7 mg/g was provided on the γ-$Al_2O_3$ having the largest surface area, verifying the importance of material surface area for achieving superior adsorption performance. The CR adsorption behaviors onto various γ-$Al_2O_3$ materials were analyzed using different kinetic models, and the results suggest a multistep adsorption mechanism. Besides, the equilibrium adsorption data well fitted the pseudo-second-order kinetic model, manifesting that the chemical adsorption process is the rate-limiting step. Moreover, the γ-$Al_2O_3$ synthesized showed good recyclability for CR removal, and thus could be a very effective and cost-saving adsorbent for the treatment of industrial wastewater containing organic pollutants.

**Keywords:** γ-$Al_2O_3$, High Surface Area, Economical Synthesis, Congo Red, Adsorption, Wastewater Treatment

## 1. Introduction

Synthetic dyestuffs are used in various manufactories for the production of rubber, paper, textile, plastics, cosmetics, etc., where a large amount of water is expended for cleaning purpose, resulting in dye-containing waste effluents [1, 2]. A variety of dyes are toxic, mutagenic, and carcinogenic, even at very minimum concentrations. Congo red (CR), a synthetic anionic azo dye, is extensively employed in textile industries. Nevertheless, exposure to excessive CR may have the potential risk of allergic reaction and anaphylactic shock. What's more, CR is resistant to biodegradation because of its complex and stable aromatic structure. Therefore, it must be removed from wastewater before being discharged into natural water bodies.

In fact, many sorts of physical and chemical techniques have been developed for the treatment of dye-contaminated wastewater. Adsorption stands on the most effective and favorable techniques because of its low cost, easy operation, high efficiency and feasible regeneration [3-5]. Different types of adsorbents have been utilized for dye removal from aqueous solutions [6, 7]. γ-$Al_2O_3$ is one of the most commonly used adsorbents owing to their large surface area, high chemical stability, nontoxicity, abundant sources, and so on [8, 9]. In addition to adsorbing dyes, γ-$Al_2O_3$ is also adaptable for the purification of other aqueous pollutants such as heavy metals [10], nitrates [11], fluorides [12], etc.

It has been recognized that the economic viability,

environmental safety, and sustainability of the developed adsorbents need to attach great importance from the perspective of mass production and large scale applications [13, 14]. Despite the fact that there are a lot of new forms of γ-$Al_2O_3$ [15] developed, most of them were synthesized using sol-gel, hydrothermal or pyrolysis methods with the addition of expensive precursors and surfactants and numerous organic solvents as well [16, 17]. In addition, harsh synthetic conditions involving high temperatures and pressures were usually required [18]. Consequently, these synthesis approaches are generally too complicated and costly and sometimes even pollutive to satisfy the economic and environmental requirements.

Precipitation is a mature technique for the production of γ-$Al_2O_3$ precursors in industry, which is featured with easy handling and cost advantage [19]. Nevertheless, the γ-$Al_2O_3$ prepared using traditional precipitation approach mostly possesses low specific surface area (< 250 $m^2$/g), small pore volume (< 0.5 $cm^3$/g) and broad pore size distributions, unfavorable to provide sufficient sites exposed for dye molecule adsorption [20]. To overcome these problems, surfactant-added precipitation methods have been introduced [21, 22]. But the high cost of some specific surfactants used for precipitation process is definitely a big drawback hindering the large scale production of alumina with superior properties. From this point, an inexpensive surfactant is of significance for promoting the commercialization of alumina production and applications. Besides, the raw materials including the aluminum and alkali sources are another important factor determining the cost of alumina synthesis using precipitation method.

Therefore, in the present study, we have adopted deliberately a cheap aluminum source, aluminum sulfate ($Al_2(SO_4)_3$), together with sodium dodecyl sulfate (SDS), which is one of the cheapest surfactants, to produce γ-$Al_2O_3$ materials through simple precipitation and subsequent calcination procedure (the reaction equations are given in Supplementary Material). It has been shown that the textural structure of the γ-$Al_2O_3$ materials can be effectively manipulated by varying the molar ratio of SDS to $Al_2(SO_4)_3$. A detail investigation on the adsorption performance of CR over the as-prepared γ-$Al_2O_3$ has been carried out. The adsorption capacity as high as 831.7 mg/g has been achieved. A parallel comparison has been made between the γ-$Al_2O_3$ synthesized and a commercial γ-$Al_2O_3$ throughout the study. The elaborative kinetic and thermodynamic analysis and reusability test results suggest that the as-prepared γ-$Al_2O_3$ materials are very promising for the treatment of CR in wastewater of industry.

# 2. Materials and Methods

### *2.1. Materials*

Aluminum sulfate ($Al_2(SO_4)_3 \cdot 18H_2O$), aqueous ammonium hydroxide ($NH_4OH$, 25 wt.%), SDS ($CH_3(CH_2)_{11}OSO_3Na$) and CR ($C_{32}H_{22}N_6O_6S_2Na_2$) were all purchased from the market. Deionized water was used in all experiments. All reagents were of chemical grade and used directly without further purification. A commercial γ-$Al_2O_3$ (denoted as Com-$Al_2O_3$) was used as a reference material for the purpose of comparative adsorption study.

### *2.2. Preparation of γ-$Al_2O_3$*

The precipitate of amorphous $Al(OH)_3$ was formed first through the reaction between $Al_2(SO_4)_3$ and $NH_4OH$ in aqueous solution. In a typical preparation procedure, 33.31 g $Al_2(SO_4)_3 \cdot 18H_2O$ (0.05 mol) and a definite amount of surfactant SDS were dissolved together in 200 mL deionized water at room temperature and stirred magnetically to obtain a homogeneous solution. The molar ratio of SDS to $Al_2(SO_4)_3 \cdot 18H_2O$ was varied from 0 to 0.75 so as to acquire the precipitates and the corresponding calcined materials with different texture structures. The precipitant $NH_3 \cdot H_2O$ solution (25 wt.%) was gradually added to the above aqueous solution to adjust pH to 9.0 along with vigorous agitation at 1500 rpm, which was operated in a vessel placed in a water bath at 75°C. The reaction mixture was further stirred for about 1 h and then aged for another 12 h without stirring. The resulted white precipitate was filtered and washed with deionized water for several times, and finally dried in oven at 100°C for 12 h to transform into pseudo boehmite. The γ-$Al_2O_3$ was obtained from pseudo boehmite powder by calcination at 600°C for 10 h in a muffle oven with a heating rate of 2°C /min. The γ-$Al_2O_3$ product is denoted as $Al_2O_3$-X (X = 0, 0.125, 0.25, 0.375, 0.5 or 0.75), where X represents the molar ratio of SDS to $Al_2(SO_4)_3$.

### *2.3. Material Characterization*

The crystal structures of the materials synthesized and the Com-$Al_2O_3$ as well were detected by an X-ray polycrystalline diffractometer (Bruker D8 Advance, Davinci) using Cu $K_\alpha$ radiation at a scanning rate ($2\theta$) of 1°$min^{-1}$ from 10° to 90°. The accelerating voltage and applied current were 40 kV and 40 mA, respectively. Data treatment of the diffraction pattern was analyzed using Jade software. The $N_2$ adsorption/desorption isotherms of various γ-$Al_2O_3$ samples were measured by cryogenic $N_2$ physisorption method on an apparatus of Micromeretics ASAP2020. Before the measurement, the sample of alumina powder was degassed at 350°C for 4 h. The specific surface area ($S_{BET}$) was calculated by using the Brunauer–Emmet–Teller (BET) equation. The pore size distribution and the total pore volume ($V_p$) were calculated from the desorption branch of the isotherm using the Barrett–Joyner–Halenda (BJH) numerical model. The morphologies of the γ-$Al_2O_3$ samples were observed on an ultra-high resolution field emission scanning electronic microscopy (SEM) instrument (NOVA Nano SEM450, FEI) using an acceleration voltage of 15 kV. The transmission electronic microscopy (TEM) investigation was conducted on a JEM-2100UHR electronic microscope (JEOL, Japan) at an accelerating voltage of 200 kV. The point of zero charge ($pH_{PZC}$) of various materials was measured by pH drift method

described in Supplementary Material. As displayed in Figure 1 and Table 1, the $pH_{PZC}$ of the samples of $Al_2O_3$-X (X = 0, 0.125, 0.25, 0.375) ranges from 4.0 to 4.7, while that of the Com-$Al_2O_3$ is 7.7.

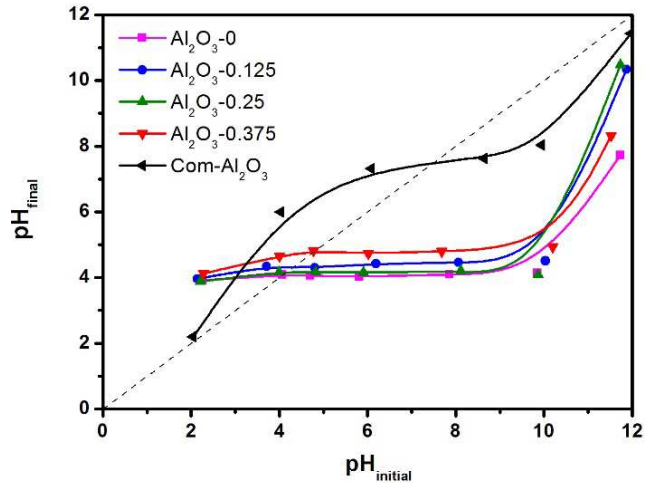


***Figure 1.*** *Plot of final pH versus initial pH of alumina suspension at 298.15 K with 0.01 mol/L NaCl solution. Dotted line represents the non-changing pH component, the calibration line.*

***Table 1.*** *The $pH_{PZC}$ of $Al_2O_3$-X and Com-$Al_2O_3$ samples.*

| Sample | $Al_2O_3$-0 | $Al_2O_3$-0.125 | $Al_2O_3$-0.25 | $Al_2O_3$-0.375 | Com-$Al_2O_3$ |
|---|---|---|---|---|---|
| $pH_{PZC}$ | 4.0 | 4.3 | 4.1 | 4.7 | 7.7 |

### *2.4. Adsorption Performance Test*

Adsorption performance of all γ-$Al_2O_3$ samples was tested in CR aqueous solution to determine the relative adsorption capacity and CR removal efficiency. Typically, 50 mg adsorbent (around 80 mesh in granular size) was added to a beaker filled with 100 mL CR aqueous solution having a CR concentration in a range of 50-800 mg/L. The suspension was stirring continuously at 25°C with a required adsorption time and the pH value was kept constant at 5.0 by adding 0.1 mol/L HCl solution. The CR concentration before and after adsorption was both measured at the maximum absorption wavelength of CR (497 nm) on a visible spectrophotometer (SDPTOP-721, Shanghai). The justification for the determination of the adsorbent amount to be 50 mg in 100 mL solution and the pH to be 5.0 was supplied in Supplementary Material.

The adsorption capacity ($q_e$, mg/g) of an adsorbent after reaching equilibrium state and the removal efficiency of CR for various $Al_2O_3$ samples were calculated using the following equations, respectively:

$$q_e = (C_0 - C_e)V / W \quad (1)$$

$$q_e = (C_0 - C_e) / C_0 \quad (2)$$

where $C_0$ and $C_e$ (mg/L) are the initial and equilibrium concentrations of CR, respectively; $V$ (L) is the volume of the solution, and $W$ (g) is the weight of the adsorbent used. The same adsorption experiment was also conducted for the sample of Com-$Al_2O_3$ which had been calcined at 600°C for 10 h beforehand.

## 3. Results and Discussion

### *3.1. Effects of SDS Molar Ratio on Textural Property and Morphology of γ-$Al_2O_3$*

The pseudo boehmite and γ-$Al_2O_3$ materials synthesized in the present work and the sample of Com-$Al_2O_3$ as well were identified by means of XRD technique, as shown in Figure 2, confirming the deserved crystal structure of each material. The main pattern of curve (a) in Figure 2 can be assigned to the pseudo boehmite structure (JCPDS No. 21-1307) of the sample. Besides, a peak appearing at $2\theta$ of 19.8° is indicative of the presence of SDS in the sample of pseudo boehmite. After calcination, all of the samples show typical γ-$Al_2O_3$ structure pattern (JCPDS No. 10-0425), and the characteristic peaks observed at $2\theta$ of 37.7°, 45.9°, 67.3° can be indexed to the (311), (400), (440) reflections of γ-$Al_2O_3$. SDS disappeared after the transformation of the pseudo boehmite to γ-$Al_2O_3$ through calcination at 600°C.

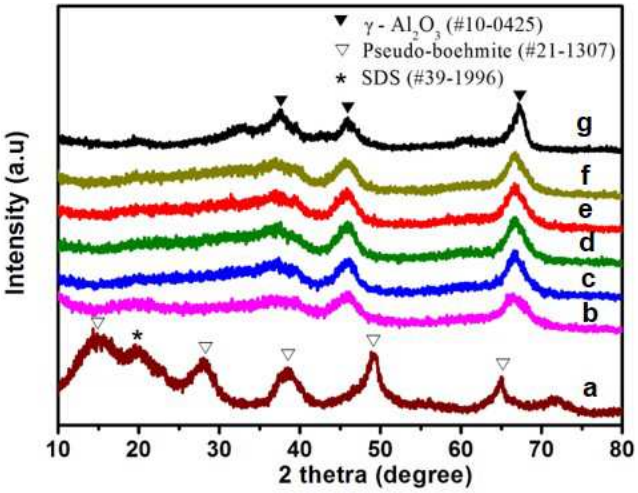


***Figure 2.*** *XRD patterns of different materials involved. (a) pseudo boehmite-0.375, (b) $Al_2O_3$-0, (c) $Al_2O_3$-0.125, (d) $Al_2O_3$-0.25, (e) $Al_2O_3$-0.375, (f) $Al_2O_3$-0.5, (g) Com-$Al_2O_3$.*

The $N_2$ adsorption-desorption isotherms and pore size distributions of various γ-$Al_2O_3$ including Com-$Al_2O_3$ are shown in Figure 3. All the samples exhibit the typical IV isotherm shape having H2 hysteresis loop (Figure 3(A)) according to the IUPAC classification, which is the characteristic of nanoporous solid involving bottleneck pores [23]. The hysteresis loop for the sample of $Al_2O_3$-0 (curve (b) in Figure 3(A)), which was transformed from the product of pseudo boehmite with no SDS addition, is remarkably smaller than that of the γ-$Al_2O_3$ derived in the presence of SDS, inferring the significant influence of SDS addition on the γ-$Al_2O_3$ texture. The corresponding pore size distributions (Figure 3(B)) reveal the pore size upshift with the increase of SDS addition amount. The Com-$Al_2O_3$, however, displays a dissimilar $N_2$ adsorption-desorption behavior, pointing to its

different textural property from that of the γ-$Al_2O_3$ prepared. As clearly shown in curve (a) of Figure 3(B), the pore size distribution of Com-$Al_2O_3$ is very broad and weak, in contrast to the relatively concentrated pore size distribution for the γ-$Al_2O_3$ prepared in the present work.

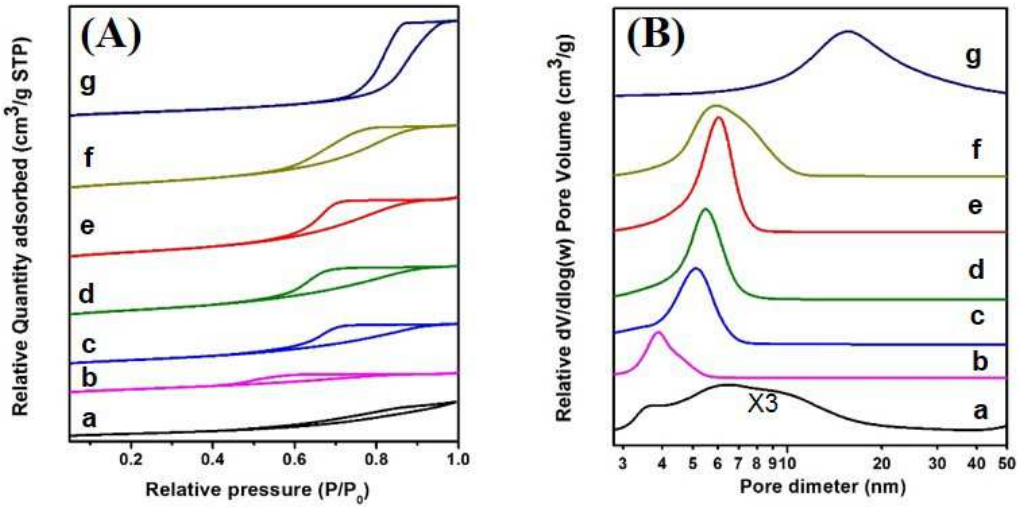


***Figure 3.*** *(A) $N_2$ adsorption-desorption isotherms and (B) corresponding pore size distributions of various alumina samples. (a) Com-$Al_2O_3$, (b) $Al_2O_3$-0, (c) $Al_2O_3$-0.125, (d) $Al_2O_3$-0.25, (e) $Al_2O_3$-0.375, (f) $Al_2O_3$-0.5, (g) $Al_2O_3$-0.75.*

Table 2 summarizes the textural properties of the γ-$Al_2O_3$ samples obtained from different molar ratio of SDS to aluminum sulfate. As can be seen, sample $Al_2O_3$-0 has the smallest pore diameter (4.5 nm) among all, and its specific surface area (267.28 $m^2$/g) and pore volume (0.29 ml/g) are also the smallest. The addition of SDS can obviously increase the average pore size, pore volume and specific surface area of the γ-$Al_2O_3$ materials. It is interesting that there is a maximum specific surface area (416.65 $m^2$/g) presented by the sample of $Al_2O_3$-0.375. Continually increasing the molar ratio of SDS, for instance, to 0.5 or 0.75, can instead decrease the specific surface area of the γ-$Al_2O_3$ obtained, although the average pore size and pore volume still grow up. By comparison with the γ-$Al_2O_3$ prepared in the presence of SDS, the material of Com-$Al_2O_3$ possesses considerably smaller specific surface area and pore volume, as given also in Table 2.

***Table 2.*** *Textural properties of γ-$Al_2O_3$ prepared with different molar ratios of SDS to aluminum sulfate and of commercial γ-$Al_2O_3$.*

| γ-$Al_2O_3$ sample | SDS molar ratio[a] | $S_{BET}$ ($m^2$/g) | $V_p$ ($cm^3$/g) | Average $d_p$ (nm) |
|---|---|---|---|---|
| $Al_2O_3$-0 | 0 | 267.28 | 0.29 | 3.8 |
| $Al_2O_3$-0.125 | 0.125 | 312.68 | 0.55 | 5.3 |
| $Al_2O_3$-0.25 | 0.25 | 389.97 | 0.70 | 5.6 |
| $Al_2O_3$-0.375 | 0.375 | 416.65 | 0.81 | 5.8 |
| $Al_2O_3$-0.5 | 0.5 | 409.10 | 0.84 | 6.0 |
| $Al_2O_3$-0.75 | 0.75 | 326.45 | 1.12 | 14.4 |
| Com-$Al_2O_3$ | - | 202.23 | 0.45 | 7.2 |

[a] The molar ratio of SDS to aluminum sulfate ($Al_2(SO_4)_3 \cdot 18H_2O$) used during precipitation.

Besides the impact on the textural property, the addition of SDS can observably influence the morphology of the resulted γ-$Al_2O_3$ materials. Figure 4 shows the SEM and TEM images of several γ-$Al_2O_3$ samples prepared through adding different SDS molar ratios. For the materials based on SDS addition, uniform and fluffy texture can be clearly observed on SEM images (Figure 4(c) and (d)), while the material without adding SDS appears to be tight and solid (Figure 4(b)). From the TEM images, one can see that for the sample of $Al_2O_3$-0.375 (Figure 4(f)) many strip-like lattice fringes are connected loosely with large voids contained, whereas the sample of $Al_2O_3$-0 (Figure 4(e)) has a compact framework structure with small pores interspersed. For the Com-$Al_2O_3$ material (Figure 4(a)), its morphology looks agglomerate, more like that of the sample of $Al_2O_3$-0 prepared in absence of SDS.

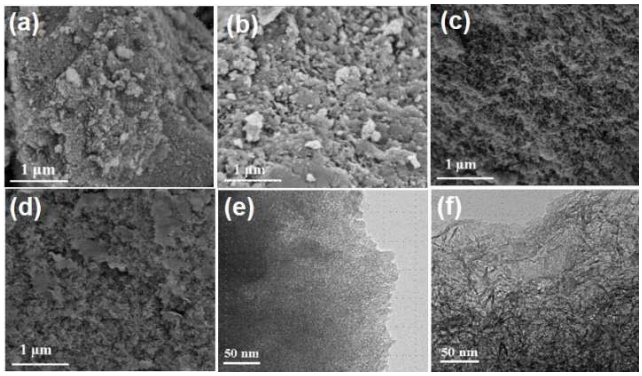


***Figure 4.*** *SEM images of alumina samples of (a) Com-$Al_2O_3$, (b) $Al_2O_3$-0, (c) $Al_2O_3$-0.25, (d) $Al_2O_3$-0.375, and the corresponding TEM images of (e) $Al_2O_3$-0, (f) $Al_2O_3$-0.375.*

Concerning the precipitation process of aluminum sulfate in absence of the surfactant SDS, the condensation reaction could occur almost simultaneously with the hydrolysis of aluminum salt as soon as adding alkali into the solution. Consequently, amorphous hydrated alumina were formed from random aggregation of huge amounts of tiny $Al(OH)_3$ precipitate particles. The $\gamma$-$Al_2O_3$ eventually obtained thus possessed a solid and irregular texture. Upon the addition of surfactant SDS, the interactions between SDS and the $Al(OH)_3$ particle surface could take into effect. As demonstrated in Figure 5, when the SDS concentration was between the first and second critical micellar concentration (CMC) [24, 25], a lot of micelles could be formed in a shape of small spheres. In this circumstance, the $Al(OH)_3$ particles produced could be effectively separated by the SDS micellar spheres owing to the mutual adsorption between two sides. As a result, serious agglomeration of the $Al(OH)_3$ precipitate could be alleviated. During the ripening process, the $Al(OH)_3$ particles were gradually transformed to pseudo boehmite structure and the SDS spheres were still dispersed evenly among them. The subsequent calcination could hence leave relatively uniform pores in the $\gamma$-$Al_2O_3$ sample due to the removal of SDS spheres. While raising the concentration of SDS exceeding the second CMC, the surfactant micelles could transfer to rod structure, which could be connected into network across the $Al(OH)_3$ precipitate and thus the pseudo boehmite body. Further increasing the SDS concentration to a high level, the SDS rods could gather in groups to form large bundles. Large intersecting pores could thereby be brought about after burning off SDS bundles. It is worthy of note that an excessive addition of SDS could utmostly expand the pore size and volume, but do harm to the specific surface area of the $\gamma$-$Al_2O_3$ produced. This may probably be associated with the formation of oversized SDS bundle assembles, which could not be well dispersed throughout the precipitate. The mechanism of SDS addition effect suggested above can be verified by the textural and morphological features of various $\gamma$-$Al_2O_3$ materials obtained with varying SDS molar ratios, as already shown in Table 2 and Figure 4.

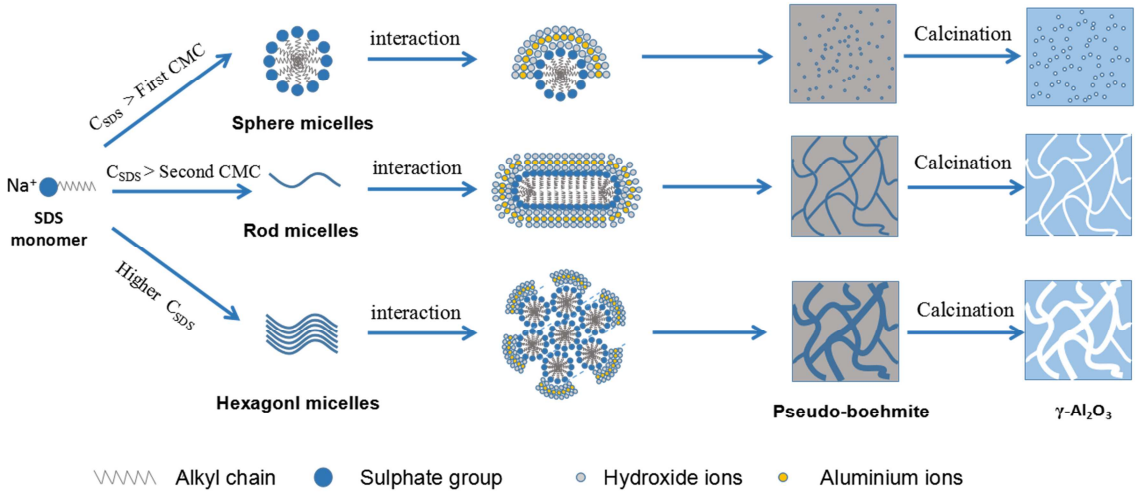


***Figure 5.*** *Transformation of SDS micelles at different concentrations and the proposed mechanism of SDS addition effect on the texture of resultant $\gamma$-$Al_2O_3$.*

### *3.2. Adsorption Kinetics of $\gamma$-$Al_2O_3$ for CR Removal*

The adsorption performance of several $\gamma$-$Al_2O_3$ samples prepared were investigated for removal of CR and compared to the result of the Com-$Al_2O_3$. The influence of initial CR concentration ($C_0$) on the adsorption capacity ($q_e$) of various $\gamma$-$Al_2O_3$ acquired after reaching each adsorption equilibrium (for 180 min) is shown in Figure 6. As can be seen, for all the samples including the Com-$Al_2O_3$, the respective adsorption capacities increase almost linearly with the initial CR concentration when it is below 300 mg/L. The maximum capacity is approached after $C_0$ exceeding 700 mg/L for every sample, and meanwhile the saturation state is achieved separately. The maximal adsorption capacity of the $Al_2O_3$-0.375 is above 800 mg/g, which is the largest one among all and also much higher than that of the Com-$Al_2O_3$ of merely around 450 mg/g.

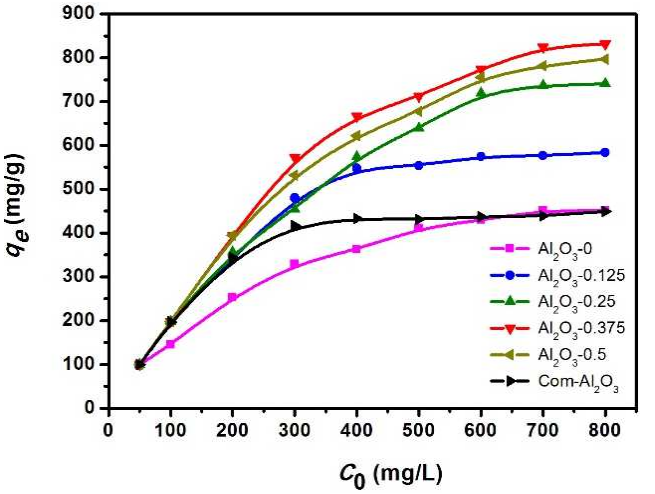


***Figure 6.*** *Adsorption capacity ($q_e$) of different $\gamma$-$Al_2O_3$ samples including Com-$Al_2O_3$ for CR removal with the change of initial CR concentration ($C_0$). Adsorption condition: T = 25°C, pH = 5.0, adsorbent dose = 50 mg, and adsorption time = 180 min.*

The adsorption amount of CR changing with the contact time of both $Al_2O_3$-0.375 and Com-$Al_2O_3$ with the solution was compared at an initial CR concentration of 300 mg/L. The kinetics of the adsorption proceeding on the two adsorbents, in particular the possible rate-limiting step, is further analyzed by fitting the models based on the pseudo-first-order, the pseudo-second-order and the intra-particle diffusion assumptions, respectively. The pseudo-first-order kinetic model was suggested by Lagergren to describe the adsorption in solid/liquid systems based on adsorption capacity [26]. The pseudo-second-order model can be applicable to the process involving chemisorption [27]. The intra-particle diffusion model is another commonly used model, which is capable of identifying the reaction pathways and adsorption mechanisms and predicting the rate-limiting step [6, 28, 29]. The linear forms of these three models are expressed by the following equations:

$$\ln(q_e - q_t) = \ln q_e - k_1 t \quad (3)$$

$$t/q_t = 1/k_2 q_e^2 + t/q_e \quad (4)$$

$$q_t = k_d t^{0.5} + C \quad (5)$$

where $q_e$ and $q_t$ (mg/g) are the amount of CR adsorbed at equilibrium and at a definite time $t$ (min), respectively, and $k_1$ ($min^{-1}$) and $k_2$ ($g \cdot mg^{-1} \cdot min^{-1}$) are the pseudo-first-order and pseudo-second-order rate constants, respectively. $k_d$ ($mg \cdot g^{-1} \cdot min^{-1/2}$) is the intra-particle diffusion rate constant and C (mg/g) is an indication of boundary layer effect of the adsorbent particles.

***Table 3.*** *Kinetic parameters derived from three different models for CR adsorption over $Al_2O_3$-0.375 and Com-$Al_2O_3$ at initial CR concentration of 300 mg/L and pH of 5.0.*

| Kinetic model | Kinetic parameter | $Al_2O_3$ -0.375 | Com -$Al_2O_3$ |
|---|---|---|---|
| Experimental result | $q_{e,exp}$ (mg $g^{-1}$) | 591.2 | 415.2 |
| Pseudo-first-order | $q_{e,cal}$ ($mg \cdot g^{-1}$) | 441.9 | 337.1 |
| | $k_1$ ($min^{-1}$) | 0.0272 | 0.0168 |
| | $R^2$ | 0.915 | 0.907 |
| Pseudo-second-order | $q_{e,cal}$ ($mg \cdot g^{-1}$) | 621.1 | 433.3 |
| | $k_2$ ($g \cdot mg^{-1} \cdot min^{-1}$) | $1.327*10^{-4}$ | $9.275*10^{-5}$ |
| | $R^2$ | 0.999 | 0.989 |
| Intraparticle diffusion | $k_{d1}$ ($mg \cdot g^{-1} \cdot min^{-1/2}$) | 46.5 | 32.1 |
| | $C_{d1}$ ($mg \cdot g^{-1}$) | 151.1 | 50.4 |
| | $R_{d1}^2$ | 0.961 | 0.973 |
| | $K_{d2}$ ($mg \cdot g^{-1} \cdot min^{-1/2}$) | 11.9 | 18.0 |
| | $C_{d2}$ ($mg \cdot g^{-1}$) | 431.1 | 153.2 |
| | $R_{d2}^2$ | 0.995 | 0.963 |
| | $K_{d3}$ ($mg \cdot g^{-1} \cdot min^{-1/2}$) | 0.6 | 4.1 |
| | $C_{d3}$ ($mg \cdot g^{-1}$) | 582.2 | 350.8 |
| | $R_{d3}^2$ | 0.979 | 0.963 |

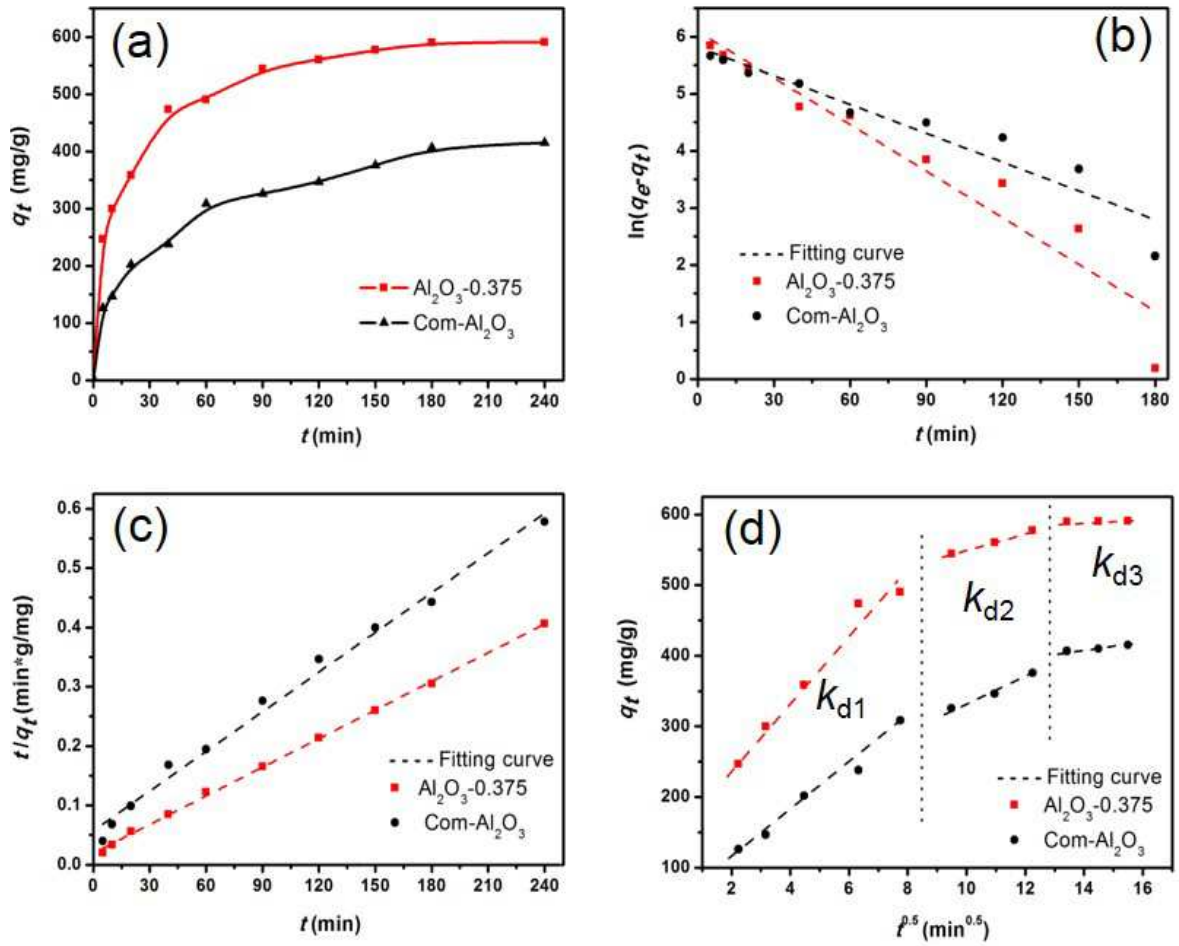


***Figure 7.*** *(a) Time dependence of CR adsorption onto $Al_2O_3$-0.375 and Com-$Al_2O_3$, and the fitting lines of (b) pseudo-first-order model, (c) pseudo-second-order model, and (d) intra-particle diffusion model. Adsorption condition: T = 25°C, pH = 5.0, adsorbent dose = 50 mg, $C_0$ = 300 mg/L.*

Figure 7(a) displays the time curves of CR adsorption on the two adsorbents, showing the steady states over both adsorbents attained after prolonging the duration of CR adsorption to more than 180 min. The fitting results of above three kinetic models are presented in Figure 7(b-d), and the kinetics parameters with each regression coefficient ($R^2$) are summarized in Table 3. The better fitting results along with the higher regression coefficients for the two γ-$Al_2O_3$ adsorbents can be gained when using the pseudo-second-order model rather than pseudo-first-order model, indicating the chemisorption role is prevalent for CR removal in both cases.

With respect to the influence of diffusion on the adsorption processes, it can be assessed using the intra-particle diffusion model. As shown in Figure 7(d), three linear parts each with definite intercept appear by fitting the plots for both adsorbents, indicating that there were three stages involved in the adsorption process. Thus, a multistep mechanism can be postulated [6, 29]. The sharp first part represents the stage of CR adsorption onto the exterior surface of γ-$Al_2O_3$ particles via film diffusion mechanism driven by high initial CR concentration and large concentration gradient. The second region refers to intra-particle diffusion. In this stage, the external adsorption sites of the γ-$Al_2O_3$ particles were mostly occupied, and the CR molecules inevitably diffused into the inner pores of the adsorbents. The last period has a flat slope, called as equilibrium stage. The intra-particle diffusion rate during this period slowed down further due to the low CR concentration in the solutions and the increasing occurrence of reversible desorption. The intra-particle diffusion rate constants for the stagewise adsorption descend in the order: $k_{d1} > k_{d2} > k_{d3}$. Furthermore, the adsorption capacity during the first stage accounted for the most amount of all, implying a dominating contribution of the external surface of the adsorbents to the CR adsorption. In contrast, the inner pores were less effective in the adsorption. Making a comparison in the value of parallel $k_d$ between the adsorbents of $Al_2O_3$-0.375 and Com-$Al_2O_3$, it can be found that the $Al_2O_3$-0.375 could provide higher $k_{d1}$ than the Com-$Al_2O_3$, manifesting a rapider rate of CR adsorption onto the external surface of $Al_2O_3$-0.375 adsorbent.

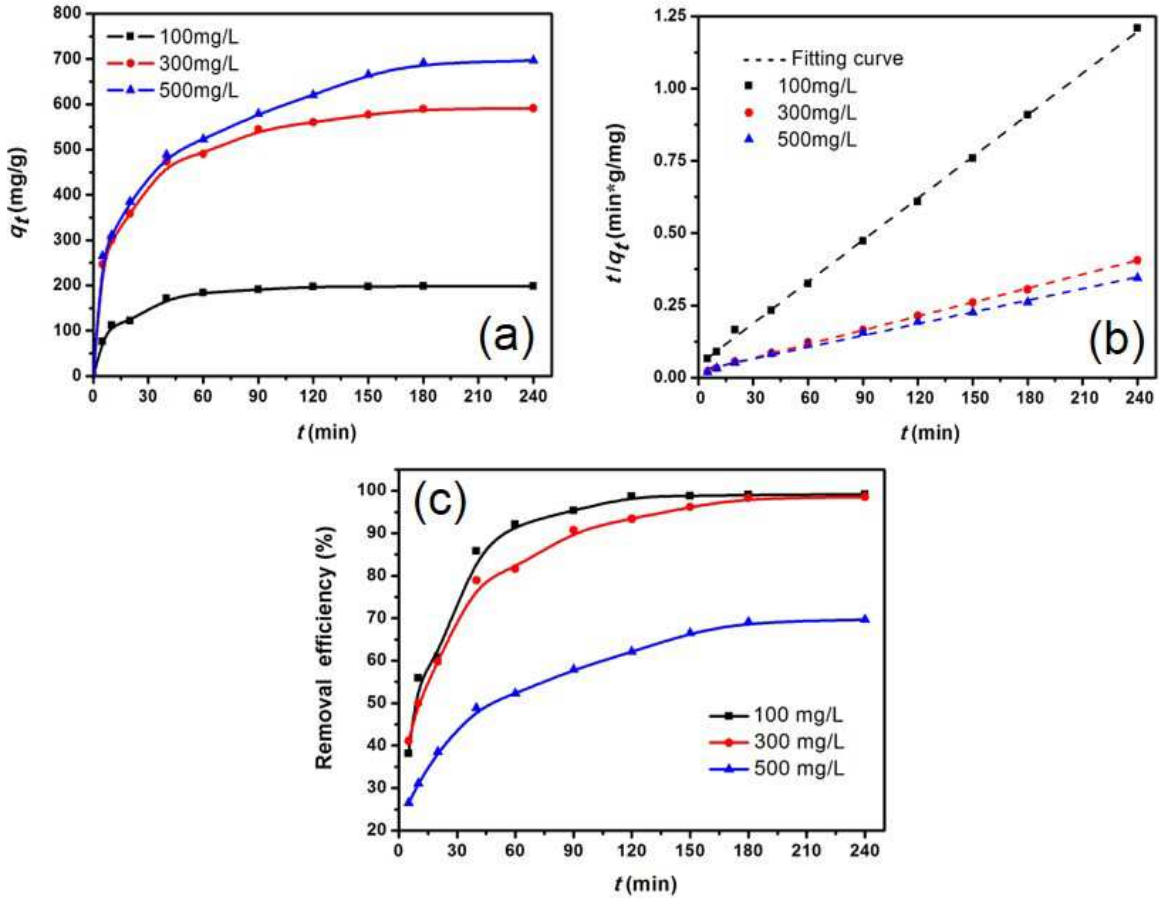


***Figure 8.*** *(a) Time curves and (b) the pseudo-second-order model fitting plots and (c) the removal efficiency for CR adsorption on $Al_2O_3$-0.375 at different initial CR concentrations. Adsorption condition: T = 25 °C, pH = 5.0, and adsorbent dose = 50 mg.*

The kinetic adsorption data on $Al_2O_3$-0.375 at different initial CR concentrations in a range of 100-500 mg/L are given in Figure 8 and the fitting parameters of pseudo-second-order model are listed in Table 4. Good fitting results and high correlation coefficients ($R^2 > 0.990$) are presented for all three kinetic adsorption curves, in agreement with the assumption of chemisorption mechanism mentioned above. Figure 8(c) displays the removal efficiency of CR over $Al_2O_3$-0.375 as a function of contact time, which changes with initial CR concentration. Removal efficiency approaching 100% can be achieved, showing

superior adsorption ability of $Al_2O_3$-0.375 in CR solution.

***Table 4.*** *Kinetic parameters and removal efficiency (in 180 min) over $Al_2O_3$-0.375 at different initial CR concentration. Adsorption condition: T = 25°C, pH = 5.0, and adsorbent dose = 50 mg.*

| CR concentration | $q_{e,exp}$ (mg $g^{-1}$) | Pseudo-second-order model | | | Removal efficiency |
|---|---|---|---|---|---|
| | | $q_{e,cal}$ (mg $g^{-1}$) | $k_2$ (g $mg^{-1}$ $min^{-1}$) | $R^2$ | |
| 100.0 mg/L | 198.4 | 207.9 | $5.300*10^{-4}$ | 0.999 | 99.2% |
| 300.0 mg/L | 591.2 | 621.1 | $1.328*10^{-4}$ | 0.999 | 98.5% |
| 500.0 mg/L | 696.4 | 723.2 | $7.843*10^{-5}$ | 0.995 | 69.6% |

### *3.3. Adsorption Isotherms and Thermodynamics of γ-$Al_2O_3$ for CR Removal*

To study the adsorption thermodynamics of various γ-$Al_2O_3$ samples prepared and the Com-$Al_2O_3$ as well, Langmuir and Freundlich equations were employed to simulate the trend of adsorption capacity changing with the concentration of CR at equilibrium state, which are expressed as follows [30].

$$C_e / q_e = 1/bq_m + C_e / q_m \quad (6)$$

$$\log q_e = \log K_f + \log C_e / n \quad (7)$$

where $q_e$ (mg/g) is the relative amount of adsorbate adsorbed at equilibrium; $C_e$ (mg/L) is the equilibrium concentration of CR in solution; $q_m$ (mg/g) is the monolayer adsorption capacity which is also the maximum of adsorption capacity; $b$ (L/mg) is the Langmuir constant or binding energy constant related to the energy of adsorption process; $K_f$ [(mg/g) $(L/mg)^{1/n}$] and $1/n$ are Freundlich constants, indicating the adsorption capacity and adsorption intensity, respectively.

Figure 9 represents the plots of the isothermal adsorption data and the fitting results based on Langmuir and Freundlich isotherm models. The isotherm parameters ($q_m$, $b$, $n$, and $K_f$) and linear correlation coefficient ($R^2$) values for each model obtained are listed in Table 5.

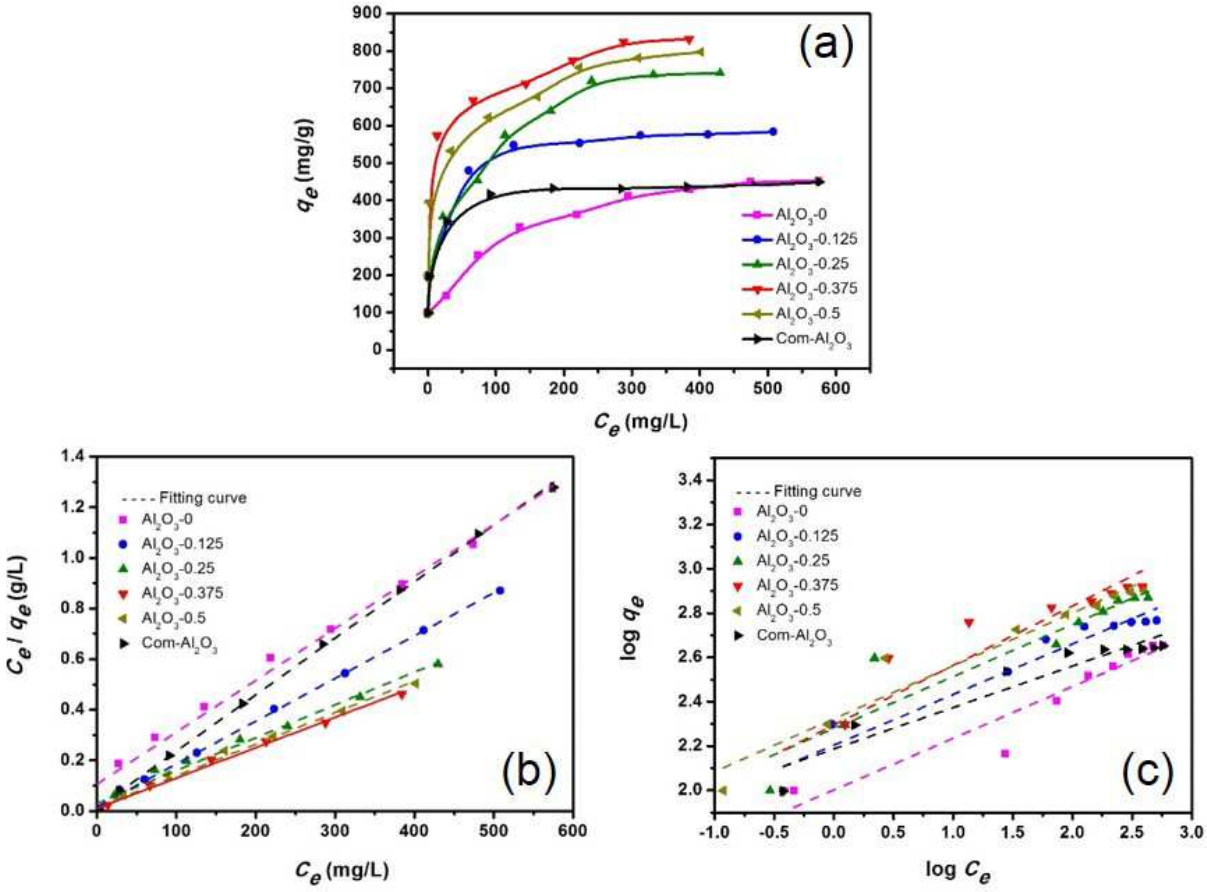


***Figure 9.*** *(a) CR adsorption isotherm curves on various alumina samples, and the fitting results based on Langmuir model (b) and Freundlich model (c). Adsorption condition: T = 25°C, pH = 5.0, adsorbent dose = 50 mg, and adsorption time = 180 min.*

Obviously, Langmuir model is more suitable with higher $R^2$ than Freundlich model for fitting the adsorption data of CR on different alumina samples. This finding indicates that the CR adsorption follows a monolayer mechanism on these adsorbents. The maximum adsorption capacity of CR on every adsorbent can be estimated from Langmuir model fitting. The

result of 833.3 mg/g obtained on $Al_2O_3$-0.375 ranks the first, also much higher than that of Com-$Al_2O_3$ with 448.4 mg/g. Because the $Al_2O_3$-0.375 owns the largest specific surface area among all, it suggests that its tremendous surface should be the main reason for the high adsorption capacity for CR removal. Indeed, for all the γ-$Al_2O_3$ samples, the maximum adsorption capacity rises almost proportionally with the increase of specific surface area, in accordance with the literature reports [1, 4].

***Table 5.*** *Adsorption isotherm parameters of Langmuir and Freundlich models.*

| Sample | Langmuir isotherm model | | | Freundlich isotherm model | | |
|---|---|---|---|---|---|---|
| | $q_{max}$ (mg/g) | $b$ (L/mg) | $R^2$ | $K_f$ (mg/g) (L/mg)$^{1/n}$ | $n$ | $R^2$ |
| $Al_2O_3$-0 | 487.8 | 0.02 | 0.987 | 100.3 | 4.3 | 0.898 |
| $Al_2O_3$-0.125 | 591.7 | 0.1 | 0.999 | 160.1 | 4.4 | 0.933 |
| $Al_2O_3$-0.25 | 769.2 | 0.04 | 0.987 | 190.0 | 4.3 | 0.865 |
| $Al_2O_3$-0.375 | 833.3 | 0.1 | 0.996 | 229.7 | 4.3 | 0.862 |
| $Al_2O_3$-0.5 | 800.0 | 0.09 | 0.994 | 210.4 | 4.2 | 0.936 |
| Com-$Al_2O_3$ | 448.4 | 0.2 | 0.999 | 153.7 | 5.3 | 0.903 |

The adsorption thermodynamic parameters such as the change in Gibb's free energy ($\Delta G^0$), entropy ($\Delta S^0$) and enthalpy ($\Delta H^0$) for adsorption of CR on the prepared $Al_2O_3$-0.375 were calculated according to the following equations [31].

$$\Delta G^0 = -RT \ln K \tag{8}$$

$$\ln K = \Delta S^0 / R - \Delta H^0 / RT \tag{9}$$

where $K$ is the adsorption equilibrium constant, which can be derived from Langmuir isotherm constant $b$ (L/mg) [29, 32]. Additionally, R is the universal gas constant (8.314 J/mol K), and $T$ is the absolute temperature (K). The thermodynamic parameters obtained are given in Table 6.

***Table 6.*** *Thermodynamic parameters for adsorption of CR onto $Al_2O_3$-0.375. Adsorption condition: T = 25°C, pH = 5.0, adsorbent dose = 50 mg, and adsorption time = 180 min.*

| Temperature (K) | $\Delta G^0$ (kJ·mol$^{-1}$) | $\Delta S^0$ (kJ·mol$^{-1}$·K$^{-1}$) | $\Delta H^0$ (kJ·mol$^{-1}$) | $R^2$ |
|---|---|---|---|---|
| 298.15 | -28.75 | | | |
| 308.15 | -31.28 | 0.25 | 46.78 | 0.999 |
| 318.15 | -33.81 | | | |

The negative value of the $\Delta G^0$ ranges from -28.75 to -33.81 kJ/mol with the temperature varying from 298.15 K to 318.15 K, indicating that the adsorption process was spontaneous and feasible, and the adsorption process became more favorable at higher temperatures. The positive value of the $\Delta H^0$ manifests the endothermic adsorption process in nature. Furthermore, the value of 46.78 kJ/mol for $\Delta H^0$ higher than 40 kJ/mol is indicative of chemical adsorption process occurring on the surface of $Al_2O_3$-0.375 [33]. The positive $\Delta S^0$ value suggests an increased randomness on the solid/solution interface during adsorption, very likely owing to the release of water molecules from binding with CR solute.

### *3.4. Possible Adsorption Mechanism*

As mentioned above, the adsorption of CR molecules onto the surface of γ-$Al_2O_3$ materials should be driven by chemical forces. A FTIR spectroscopy investigation was made to unveil the interaction between the adsorbent and the adsorbate. Figure 10 exhibits the FTIR spectra of pure CR, and the $Al_2O_3$-0.375 before and after CR adsorption. The absorption bands of pristine $Al_2O_3$-0.375 at 3441 cm$^{-1}$ and 1635 cm$^{-1}$, corresponding to the stretching vibrations of O-H groups on the surface, both decrease in intensity and shift to lower wave numbers (3428 cm$^{-1}$ and 1628 cm$^{-1}$) after CR adsorption. In the meantime, the bands of CR observed at 3458 cm$^{-1}$ and 1580 cm$^{-1}$, attributed to the stretching vibrations of N–H and –N=N–, respectively, are also diminished after adsorption, indicating the hydrogen bond formation between the hydroxyl groups of $Al_2O_3$-0.375 and the –$NH_2$ / –N=N– group of dye molecules [34]. Besides, two new peaks at 2915 cm$^{-1}$ and 2840 cm$^{-1}$, which have been assigned to the aromatic C-H stretching vibrations of CR molecule, are observed in the spectrum of CR-adsorbed $Al_2O_3$-0.375 sample in contrast to that of pristine $Al_2O_3$-0.375, confirming the real adsorption of CR on the surface of the adsorbent. Moreover, the strong bands assigned to the symmetric stretching vibration (1062 and 1121 cm$^{-1}$) and the asymmetric stretching vibration (1175 and 1225 cm$^{-1}$) of sulfonate groups of CR shift, broaden, and reduce after adsorption, evidencing the interactions between the adsorbed dye and the adsorbent through the sulfonate groups [35]. Overall, the –$NH_2$, –N=N– and –$SO_3^-$ groups of CR may be all involved in the adsorption process. It should be noted that at pH = 5.0 which was slightly higher than the $pH_{PZC}$ of $Al_2O_3$-0.375 (4.7), the adsorbent surface might appear in anionic form in aqueous solution, while CR existed also as a anion ($NH_2$–CR–$SO_3^-$) in view of its p$K_a$ value (ca. 4.1 at 25°C). As a consequence, the electrostatic interaction weakly exerted between CR and $Al_2O_3$-0.375, although it is possible that the bare $Al^{3+}$ sites on the surface can trap the sulfonate groups of CR. On the other hand, hydrogen bonding between the amino group of CR and the negatively charged –OH groups of $Al_2O_3$ and between the negative –$SO_3^-$ groups of CR and the Bronsted acid sites of $Al_2O_3$ could be formed, suggesting the dominant role of hydrogen bonding during adsorption.

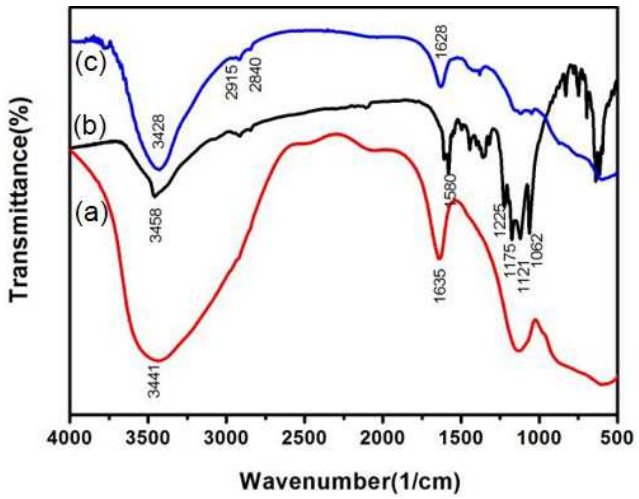


***Figure 10.*** *FTIR spectra of (a) pristine $Al_2O_3$-0.375, (b) CR, and (c) $Al_2O_3$-0.375 after adsorption.*

### *3.5. Recyclability of γ-$Al_2O_3$ Prepared*

The recyclability of an adsorbent is very important from the perspectives of economy and waste management [36]. To study the regeneration feasibility, the $Al_2O_3$-0.375 sample after CR adsorption was collected by filtration and regenerated by calcining in air at 600°C for 1 h to remove the adsorbed CR [37]. The regenerated sample was tested again for CR adsorption, and the adsorption-regeneration process was repeated following the above steps. As shown in Figure 11, no decrease in the CR removal efficiency is observed until the 6th cycle run. At the 8th cycle, the removal efficiency remained above 90%, indicating a good recyclability of the $Al_2O_3$-0.375 material.

A comparison between the $Al_2O_3$-0.375 prepared in the present work and the $Al_2O_3$ and other adsorbents reported in the literatures is made in Table 7 in the aspect of the maximum adsorption capacity for CR removal from aqueous solution. Outstanding result is presented by the $Al_2O_3$-0.375. It should be emphasized here that the $Al_2O_3$-0.375 was produced by utilizing a simple precipitation method with cheap raw materials. Therefore, this material is extremely promising to be applied for CR removal from wastewater in industry.

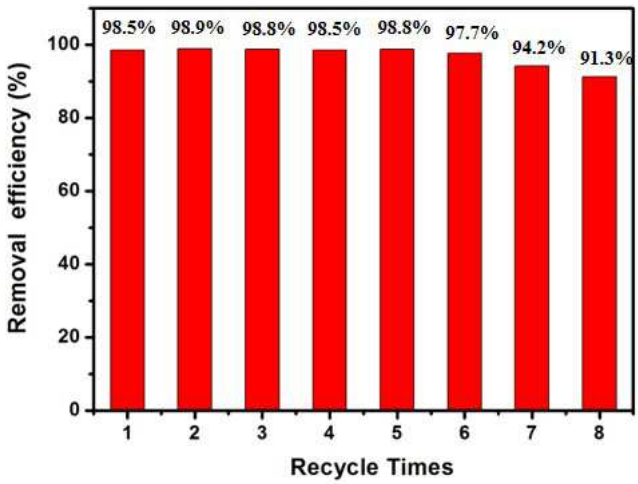


***Figure 11.*** *CR removal efficiency of the $Al_2O_3$-0.375 sample after each recycle. Adsorption condition: T = 25°C, pH = 5.0, adsorbent dose = 50 mg, adsorption time = 180 min, and $C_0$ = 300 mg/L.*

***Table 7.*** *Comparison in CR adsorption capacity of different adsorbents.*

| Adsorbent | $S_{BET}$ ($m^2 \cdot g^{-1}$) | $T$ (°C) | pH | Time (h) | $q_{max}$ ($mg \cdot g^{-1}$) | Reference |
|---|---|---|---|---|---|---|
| $Al_2O_3$-0.375 | 416.65 | 25 | 5.0 | 3 | 831.7 | This work |
| Com-$Al_2O_3$ | 202.23 | 25 | 5.0 | 3 | 449.6 | This work |
| γ-$Al_2O_3$ nanorod | 163.2 | RT | / | 12 | 416.7 | [38] |
| Hollow γ-$Al_2O_3$ microsphere | 317.8 | RT | 7.0 | 5 | 690.0 | [39] |
| Flower-like NiO | 107 | 30 | / | 3 | 534.8 | [40] |
| ZnO microsphere | 57 | 30 | 7.0 | 15 | 334.0 | [41] |
| $ZrO_2$ hollow sphere | 136 | 30 | 7 | 24 | 59.5 | [42] |
| MgO-GO microsphere | 108.7 | 30 | 6-7 | 3 | 237.0 | [43] |
| GO/chitosan fibers | 14.7 | 20 | 5.0 | 24 | 227.3 | [44] |
| ZnO-$SiO_2$ nanosphere | 46.5 | 30 | / | 24 | 90.1 | [45] |
| ZnO-NiO hollow microsphere | 130 | 30 | / | 12 | 518.0 | [46] |
| $SiO_2$-AlOOH nanosheet | 140 | 25 | 7.0 | 12 | 104.0 | [47] |
| Hydroxyapatite/chitosan | / | RT | 7.0 | 8 | 769.0 | [48] |

## 4. Conclusion

A high surface area γ-$Al_2O_3$ material has been prepared from cheap inorganic aluminum precursor by a facile and economical precipitation method in presence of inexpensive anionic surfactant SDS. By varying concentration of SDS in the solution, γ-$Al_2O_3$ with regular textural properties has been obtained, and the maximum surface area (416.65 $m^2$/g) has been provided with a molar ratio of SDS/aluminum precursor being 0.375. The CR adsorption experiments have identified that the adsorption capacities of all adsorbent samples changing with CR solution contact time well fit the pseudo-second-order kinetics model. An analysis made by use of intra-particle diffusion model reveals that the whole adsorption process is controlled by a multistep adsorption mechanism. The adsorption isotherms on both the high surface area γ-$Al_2O_3$ prepared and the commercial γ-$Al_2O_3$ obey the Langmuir model. The saturated adsorption capacity of them has been estimated to be 833.3 mg/g and 448.4 mg/g, respectively, indicating that the as-prepared γ-$Al_2O_3$ has bigger adsorption capacity than that of the commercial sample.

Besides, the present γ-$Al_2O_3$ can be reused many times with high CR removal efficiency. The combined superiority of the simple and economical preparation, high adsorption capacity and good recyclability makes the high surface area γ-$Al_2O_3$ prepared very competitive in the field of wastewater reclamation.

## Supplementary Material

Reaction equation

The chemical reactions occurring during the precipitation and drying processes are expressed as following equations [49]:

$$Al_2(SO_4)_3 + 6NH_4OH \rightarrow 2Al(OH)_3 + 3(NH_4)_2SO_4 \quad (10)$$

$$Al(OH)_3 \rightarrow AlOOH \cdot nH_2O + H_2O, \ n=0.08\text{-}0.62 \quad (11)$$

Point of zero charge ($pH_{PZC}$) of $Al_2O_3$ materials

The point of zero charge ($pH_{pzc}$) is one of the most important characteristics of an oxide surface which corresponds to the pH value of the liquid surrounding oxide particles when the sum of surface positive charges balances the sum of surface negative charges [50]. In the present study, the $pH_{PZC}$ of various materials was measured by use of the pH drift method [6]. In detail, a series of 0.01 mol/L NaCl solutions with 50 ml were adjusted to different initial pH values of 2 to 12 ($pH_{initial}$) monitored with a pH meter (PHS-3E, INESA) using 0.1 mol/L NaOH or 0.1 mol/L HCl solution. Then, an $Al_2O_3$ sample was divided into several portions, each with 100 mg was added individually to the above solutions, and every suspension obtained was continually shaken under 250 rpm at 25 °C. After 48 h, the final pH ($pH_{final}$) of every suspension was recorded and plotted against initial pH. The intersection point of the curve with the line passing the origin, i.e., when $pH_{final} = pH_{initial}$, gives the value of $pH_{PZC}$, as shown in Figure 1. The $pH_{pzc}$ of commercial $Al_2O_3$ is 7.7, and the prepared $Al_2O_3$ samples all own lower $pH_{pzc}$ value around 4.0 – 4.7 (Table 1) due to a little of sulfate ion from $Al_2(SO_4)_3$ left on $Al_2O_3$ surface after calcination [51].

Effects of adsorbent dosage and solution pH

The amount of the adsorbents used for the following adsorption performance test was determined to be 50 mg in 100 mL solution on the basis of experimental investigation into the influence of adsorbent dosage. As shown in Figure 12, the adsorption capacity of the sample $Al_2O_3$-0.375 decreased with increasing its dosage, while the change of CR removal efficiency was quite the contrary. Therefore, the proper dosage set as 0.5 g/L was a compromise between these two aspects.

In addition, the pH value was determined to be 5.0 for carrying out the adsorption experiment based on a comprehensive consideration of the $pH_{PZC}$ of $Al_2O_3$ adsorbents (4.0 – 4.7) and the $pK_a$ of CR (ca. 4.1 at 25°C) [52]. As shown in Figure 13, the adsorption capacity of all $Al_2O_3$ samples was incremental along with the decrease in pH from 10 to 5,. However, further reducing the pH of solution (pH ≤ 4.1) could cause a change in CR color from red to dark blue owing to the protonation of CR [29]. As a consequent, a deviation with respect to the relationship between the CR concentration and the photo-absorbency could appear due to the shift of maximum absorption wavelength of CR [29].

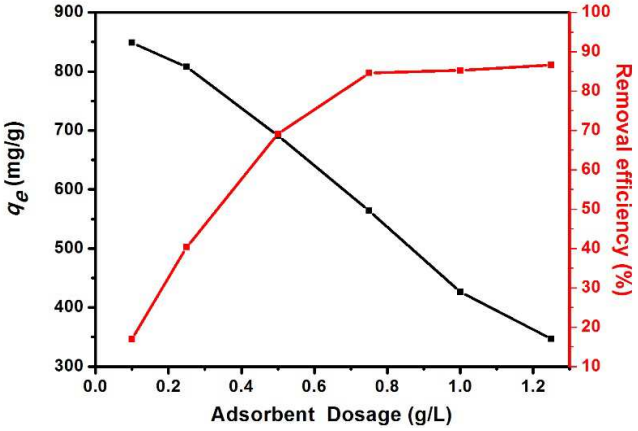


***Figure 12.*** *Adsorption capacities of the $Al_2O_3$-0.375 for CR removal with the changes of adsorbent dosage. Adsorption condition: T = 25°C, pH = 5.0, $C_0$ = 500 mg/L, and adsorption time = 180 min.*

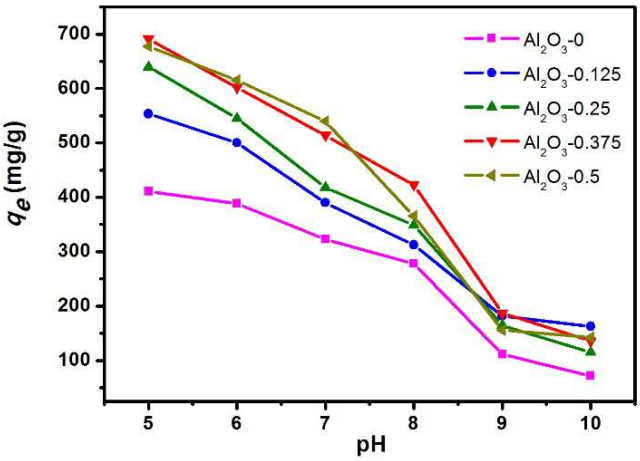


***Figure 13.*** *Adsorption capacities of the prepared $Al_2O_3$ samples for CR removal with the changes of solution pH. Adsorption condition: T = 25°C, $C_0$ = 500 mg/L, adsorbent dose = 50 mg and adsorption time = 180 min.*

Role of SDS addition

With regard to the role of SDS in the formation of large surface area and massive pore volume of the γ-$Al_2O_3$ materials, it is undoubtedly associated with its surfactant function during precipitation. SDS is a widely used amphipathic anionic surfactant in industry, having a negatively charged head group in its monomer, which can interact with inorganic species through electrostatic force. What's more, SDS can play a role of structure-directing agent in the process of inorganic material synthesis implemented in liquid phase. It is known that surfactant tends to form micelles in aqueous solution at a characteristic concentration named critical micellar concentration (CMC), and the structure of micelles in water may change from single molecules to spherical, rod and hexagonal shapes in sequence with increase in surfactant concentration or in the presence of salts [53]. Surfactant molecules self-assemble to spherical micelles above critical

micelle concentration (first CMC), which can transit to rod-like micelles at second critical micelle concentration (second CMC). It needs to be mentioned that the concentration of SDS used in this study (0.03~0.187 mol/L) is much higher than the first CMC value of SDS (0.008 mol/L) [24]. Hence it may be assumed that the SDS micelles were already formed in the precursor solution. The second CMC value of SDS in aqueous solution was reported to be 0.06 mol/L [54]. In the case of salt existing, e.g., the trivalent aluminum ions in the present study, the transition of SDS micelles from spherical to rod-like shape can occur at lower surfactant concentration than in simple surfactant solution [55]. Figure 5 illustrates schematically the transformation of SDS micelles at different concentrations and the subsequent influence on the texture of resultant γ-$Al_2O_3$ material.

## Acknowledgements

The authors are grateful to the support from PetroChina Company Ltd. grand science and technology special project (2016E-0706).

## References

[1] M. T. Yagub, T. K. Sen, S. Afroze, H. M. Ang, Dye and its removal from aqueous solution by adsorption: a review, *Advances in Colloid and Interface Science*. Vol. 209, No. 7, 2014, pp. 172-184.

[2] V. Katheresan, J. Kansedo, S. Y. Lau, Efficiency of various recent wastewater dye removal methods: A review, *Journal of Environmental Chemical Engineering*. Vol. 6, No. 2018, pp. 4676-4697.

[3] K. B. Tan, M. Vakili, B. A. Horri, P. E. Poh, A. Z. Abdullah, B. Salamatinia, Adsorption of dyes by nanomaterials: Recent developments and adsorption mechanisms, *Separation and Purification Technology*. Vol. 150, No. 2015, pp. 229-242.

[4] C. Santhosh, V. Velmurugan, G. Jacob, S. K. Jeong, A. N. Grace, A. Bhatnagar, Role of nanomaterials in water treatment applications: A review, *Chemical Engineering Journal*. Vol. 306, No. 2016, pp. 1116-1137.

[5] Y. Wang, L. Zhao, J. Hou, H. Peng, J. Wu, Z. Liu, X. Guo, Kinetic, isotherm, and thermodynamic studies of the adsorption of dyes from aqueous solution by cellulose-based adsorbents, *Water Science and Technology*. Vol. 77, No. 11, 2018, pp. 2677-2708.

[6] S. Debnath, A. Maity, K. Pillay, Impact of process parameters on removal of Congo red by graphene oxide from aqueous solution, *Journal of Environmental Chemical Engineering*. Vol. 2, No. 1, 2014, pp. 260-272.

[7] G. H. Zhao, Y. Y. Fang, W. Dai, N. Ma, Highly enhanced adsorption of congo red by functionalized finger-citron-leaf-based porous carbon, *Water Science & Technology A Journal of the International Association on Water Pollution Research*. Vol. 77, No. 1-2, 2018, pp. 220-228.

[8] W. Cai, J. Yu, M. Jaroniec, Template-free synthesis of hierarchical spindle-like γ-$Al_2O_3$ materials and their adsorption affinity towards organic and inorganic pollutants in water, *Journal of Materials Chemistry*. Vol. 20, No. 22, 2010, pp. 4587-4594.

[9] N. K. Renuka, A. V. Shijina, A. K. Praveen, Mesoporous γ-alumina nanoparticles: Synthesis, characterization and dye removal efficiency, *Materials Letters*. Vol. 82, No. 2012, pp. 42-44.

[10] A. Bhat, G. B. Megeri, C. Thomas, H. Bhargava, C. Jeevitha, S. Chandrashekar, G. M. Madhu, Adsorption and optimization studies of lead from aqueous solution using γ-alumina, *Journal of Environmental Chemical Engineering*. Vol. 3, No. 1, 2015, pp. 30-39.

[11] S. Jain, A. Bansiwal, R. B. Biniwale, S. Milmille, S. Das, S. Tiwari, P. Siluvai Antony, Enhancing adsorption of nitrate using metal impregnated alumina, *Journal of Environmental Chemical Engineering*. Vol. 3, No. 4, 2015, pp. 2342-2349.

[12] D. J. Kang, X. L. Yu, M. F. Ge, M. Y. Lin, X. Q. Yang, Y. Y. Jing, Insights into adsorption mechanism for fluoride on cactus-like amorphous alumina oxide microspheres, *Chemical Engineering Journal*. Vol. 345, No. 2018, pp. 252-259.

[13] V. K. Gupta, Suhas, Application of low-cost adsorbents for dye removal--a review, *Journal of Environmental Management*. Vol. 90, No. 8, 2009, pp. 2313-2342.

[14] S. D. Gisi, G. Lofrano, M. Grassi, M. Notarnicola, Characteristics and adsorption capacities of low-cost sorbents for wastewater treatment: A review, *Sustainable Materials and Technologies*. Vol. 9, No. 2016, pp. 10-40.

[15] Y. M. Sun, H. Wang, P. Li, X. Z. Duan, J. Xu, Y. F. Han, Synthesis and identification of hierarchical γ-AlOOH self-assembled by nanosheets with adjustable exposed facets, *CrystEngComm.* Vol. 18, No. 24, 2016, pp. 4546-4554.

[16] W. Wu, Z. J. Wan, W. Chen, M. M. Zhu, D. K. Zhang, Synthesis of mesoporous alumina with tunable structural properties, *Microporous and Mesoporous Materials*. Vol. 217, No. 2015, pp. 12-20.

[17] Y. Li, J. Su, R. Li, Preparation and characterization of super-microporous alumina with crystalline structure, *Microporous and Mesoporous Materials*. Vol. 243, No. 2017, pp. 9-15.

[18] G. Li, Y. Liu, C. Liu, Solvothermal synthesis of gamma aluminas and their structural evolution, *Microporous and Mesoporous Materials*. Vol. 167, No. 3, 2013, pp. 137-145.

[19] W. Y. Wang, K. Zhang, Y. Q. Yang, H. Liu, Z. Q. Qiao, H. A. Luo, Synthesis of mesoporous $Al_2O_3$ with large surface area and large pore diameter by improved precipitation method, *Microporous and Mesoporous Materials*. Vol. 193, No. 2014, pp. 47-53.

[20] X. Xu, Q. Yu, Z. Lv, J. Song, M. He, Synthesis of high-surface-area rod-like alumina materials with enhanced Cr(VI) removal efficiency, *Microporous and Mesoporous Materials*. Vol. 262, No. 2018, pp. 140-147.

[21] J. Čejka, Organized mesoporous alumina: synthesis, structure and potential in catalysis, *Applied Catalysis A General*. Vol. 254, No. 2, 2003, pp. 327-338.

[22] C. Márquez-Alvarez, N. Žilková, J. Pérez-Pariente, J. Čejka, Synthesis, characterization and catalytic applications of organized mesoporous aluminas, *Catalysis Reviews*. Vol. 50, No. 2, 2008, pp. 222-286.

[23] M. Thommes, K. A. Cychosz, Physical adsorption characterization of nanoporous materials: progress and challenges, *Adsorption*. Vol. 20, No. 2014, pp. 233-250.

[24] M. Miura, M. Kodama, The second CMC of the aqueous solution of sodium dodecyl sulfate. I. Conductivity, *Bulletin of the Chemical Society of Japan*. Vol. 45, No. 1972, pp. 428-431.

[25] A. P. Romani, A. E. Machado, N. Hioka, D. Severino, M. S. Baptista, L. Codognoto, M. R. Rodrigues, H. P. de Oliveira, Spectrofluorimetric determination of second critical micellar concentration of SDS and SDS/Brij 30 systems, *Journal of Fluorescence*. Vol. 19, No. 2, 2009, pp. 327-332.

[26] W. Plazinski, W. Rudzinski, A. Plazinska, Theoretical models of sorption kinetics including a surface reaction mechanism: A review, *Advances in Colloid and Interface Science*. Vol. 152, No. 1, 2009, pp. 2-13.

[27] Y. S. Ho, Review of second-order models for adsorption systems, *Journal of Hazardous Materials*. Vol. 136, No. 3, 2006, pp. 681-689.

[28] S. S. Gupta, K. G. Bhattacharyya, Kinetics of adsorption of metal ions on inorganic materials: A review, *Advances in Colloid and Interface Science*. Vol. 162, No. 1, 2011, pp. 39-58.

[29] N. T. Hai, S. J. You, A. Hosseini-Bandegharaei, H. P. Chao, Mistakes and inconsistencies regarding adsorption of contaminants from aqueous solutions: A critical review, *Water Research*. Vol. 120, No. 1, 2017, pp. 88-116.

[30] K. Y. Foo, B. H. Hameed, Insights into the modeling of adsorption isotherm systems, *Chemical Engineering Journal*. Vol. 156, No. 1, 2010, pp. 2-10.

[31] K. M. Doke, E. M. Khan, Adsorption thermodynamics to clean up wastewater; critical review, *Reviews in Environmental Science & Bio/technology*. Vol. 12, No. 1, 2013, pp. 25-44.

[32] S. K. Milonjic, A consideration of the correct calculation of thermodynamic parameters of adsorption, *Journal of the Serbian Chemical Society*. Vol. 72, No. 12, 2007, pp. 1363-1367.

[33] C.-Y. Shiau, C. C. Pan, Adsorption of basic dyes from aqueous solution by various adsorbents, *Separation Science and Technology*. Vol. 39, No. 8, 2004, pp. 1733-1750.

[34] S. Liu, Y. Ding, P. Li, K. Diao, X. Tan, F. Lei, Y. Zhan, Q. Li, B. Huang, Z. Huang, Adsorption of the anionic dye Congo red from aqueous solution onto natural zeolites modified with N,N-dimethyl dehydroabietylamine oxide, *Chemical Engineering Journal*. Vol. 248, No. 2014, pp. 135-144.

[35] S. X. Yang, L. Y. Wang, X. D. Zhang, W. J. Yang, G. L. Song, Enhanced adsorption of Congo red dye by functionalized carbon nanotube/mixed metal oxides nanocomposites derived from layered double hydroxide precursor, *Chemical Engineering Journal*. Vol. 275, No. 2015, pp. 315-321.

[36] N. B. Singh, G. Nagpal, S. Agrawal, Rachna, Water purification by using Adsorbents: A review, *Environmental Technology & Innovation*. Vol. 11, No. 2018, pp. 187-240.

[37] V. Vimonses, S. M. Lei, J. Bo, C. W. K. Chow, C. Saint, Adsorption of congo red by three Australian kaolins, *Applied Clay Science*. Vol. 43, No. 3, 2009, pp. 465-472.

[38] X. Liu, C. Niu, X. Zhen, J. Wang, X. Su, Novel approach for synthesis of boehmite nanostructures and their conversion to aluminum oxide nanostructures for remove Congo red, *Journal of Colloid and Interface Science*. Vol. 452, No. 2015, pp. 116-125.

[39] J. Y. Tian, P. Tian, H. C. Pang, G. L. Ning, R. F. Bogale, H. Cheng, S. W. Shen, Fabrication synthesis of porous $Al_2O_3$ hollow microspheres and its superior adsorption performance for organic dye, *Microporous and Mesoporous Materials*. Vol. 223, No. 2016, pp. 27-34.

[40] Y. Q. Zheng, B. C. Zhu, H. Chen, Y. Wei, C. J. Jiang, J. G. Yu, Hierarchical flower-like nickel (II) oxide microspheres with high adsorption capacity of Congo red in water, *Journal of Colloid and Interface Science*. Vol. 504, No. 2017, pp. 688-696.

[41] C. Lei, M. Pi, C. Jiang, B. Cheng, J. Yu, Synthesis of hierarchical porous zinc oxide (ZnO) microspheres with highly efficient adsorption of Congo red, *Journal of Colloid and Interface Science*. Vol. 490, No. 2017, pp. 242-251.

[42] C. Wang, Y. Le, B. Cheng, Fabrication of porous $ZrO_2$ hollow sphere and its adsorption performance to Congo red in water, *Ceramics International*. Vol. 40, No. 7, 2014, pp. 10847-10856.

[43] J. Xu, D. F. Xu, B. C. Zhu, B. Cheng, C. J. Jiang, Adsorptive removal of an anionic dye Congo red by flower-like hierarchical magnesium oxide (MgO)-graphene oxide composite microspheres, *Applied Surface Science*. Vol. 435, No. 2018, pp. 1136-1142.

[44] Q. J. Du, J. K. Sun, Y. H. Li, X. X. Yang, X. H. Wang, Z. H. Wang, L. H. Xia, Highly enhanced adsorption of congo red onto graphene oxide/chitosan fibers by wet-chemical etching off silica nanoparticles, *Chemical Engineering Journal*. Vol. 245, No. 6, 2014, pp. 99-106.

[45] J. J. Zhang, X. L. Yan, M. Q. Hu, X. Y. Hu, M. Zhou, Adsorption of Congo red from aqueous solution using ZnO-modified $SiO_2$ nanospheres with rough surfaces, *Journal of Molecular Liquids*. Vol. 249, No. 2018, pp. 772-778.

[46] C. S. Lei, M. Pi, B. Cheng, C. J. Jiang, J. Q. Qin, Fabrication of hierarchical porous ZnO/NiO hollow microspheres for adsorptive removal of Congo red, *Applied Surface Science*. Vol. 435, No. 2018, pp. 1002-1010.

[47] Z. L. Yan, L. J. Fu, H. M. Yang, J. Ouyang, Amino-functionalized hierarchical porous $SiO_2$ -AlOOH composite nanosheets with enhanced adsorption performance, *Journal of Hazardous Materials*. Vol. 344, No. 2018, pp. 1090-1100.

[48] H. J. Hou, R. H. Zhou, P. Wu, L. Wu, Removal of Congo red dye from aqueous solution with hydroxyapatite/chitosan composite, *Chemical Engineering Journal*. Vol. 211-212, No. 22, 2012, pp. 336-342.

[49] P. Raybaud, M. Digne, R. Iftimie, W. Wellens, P. Euzen, H. Toulhoat, Morphology and surface properties of boehmite (γ-AlOOH): A density functional theory study, *Journal of Catalysis*. Vol. 201, No. 2, 2001, pp. 236-246.

[50] J. P. Reymond, F. Kolenda, Estimation of the point of zero charge of simple and mixed oxides by mass titration, *Powder Technology*. Vol. 103, No. 1, 1999, pp. 30-36.

[51] S. I. Kim, S. I. Woo, Characterization of alumina modified with sulfate and phosphate, *Korean Journal of Chemical Engineering*. Vol. 8, No. 3, 1991, pp. 177-182.

[52] I. M. Ahmed, M. S. Gasser, Adsorption study of anionic reactive dye from aqueous solution to Mg–Fe–$CO_3$ layered double hydroxide (LDH), *Applied Surface Science*. Vol. 259, No. 42, 2012, pp. 650-656.

[53] N. Kataria, V. K. Garg, Removal of Congo red and Brilliant green dye from aqueous solution using flower shaped ZnO nanoparticles, *Journal of Environmental Chemical Engineering*. Vol. 5, No. 6, 2017, pp. 5420-5428.

[54] A. P. Romani, A. E. D. H. Machado, N. Hioka, D. Severino, M. S. Baptista, L. Codognoto, M. R. Rodrigues, H. P. M. D. Oliveira, Spectrofluorimetric Determination of Second Critical Micellar Concentration of SDS and SDS/Brij 30 Systems, *Journal of Fluorescence*. Vol. 19, No. 2, 2009, pp. 327-332.

[55] R. G. Alargova, K. D. Danov, J. T. Petkov, P. A. Kralchevsky, G. Broze, A. Mehreteab, Sphere-to-Rod transition in the shape of anionic surfactant micelles determined by surface tension measurements, *Langmuir*. Vol. 13, No. 21, 1997, pp. 5544-5551.